3-D Measurement of Body Tissues Based on Ultrasound Images with 3-D Spatial Information

Qing Hua Huang[1], Yong Ping Zheng[1], Robert Li[2], and Min Hua Lu[1]

1. Department of Health Technology and Informatics, The Hong Kong Polytechnic University, Kowloon, Hong Kong SAR, China

2. Department of Diagnostic Radiology, St Paul's Hospital, Hong Kong SAR, China

Running Title: **Ultrasound Measurement with 3-D Spatial Information**

Corresponding author:

Yongping Zheng, PhD.

Department of Health Technology and Informatics,

The Hong Kong Polytechnic University,

Hung Hom, Kowloon, Hong Kong SAR, P.R.China

Tel: 852-27667664

Fax: 852-23624365

Email: ypzheng@ieee.org

Abstract

In this study, we developed a new method to perform 3-D measurements between the recorded B-scans using the corresponding spatial location and orientation of each B-scan without the need to create a 3-D volume. A portable ultrasound scanner and an electromagnetic spatial locator attached to the US probe were used. During data collection, the ultrasound probe was moved over the region of interest. A small number of B-scans containing ***interested*** anatomical information were captured from different body parts and displayed in a 3-D space with their corresponding locations recorded by the spatial locator. In the B-scan planes, the distance between any two points as well as the angle between any two lines could be calculated. In validation experiments, three distances and three angles of a custom-designed phantom were measured using this method. In comparison with the results measured by a micrometer, the mean error of distance measurement was -0.8±1.7 mm (-2.3±3.6%) and that of angle measurement was -0.3±2.9° (-0.1±4.1%). The lengths of the first metatarsals and the angles between the first metatarsals and the middle part of the tibias of three subjects were measured *in vivo* using MRI and the ultrasound method by two operators before and after MRI scanning. The overall percentage differences of the length and angle measurements were 0.8±2.2% and 2.5±3.6%, respectively. The results showed that this ultrasound method had good repeatability and reproducibility (ICC values > 0.75). We expect that this new method could potentially provide a quick and effective approach for the 3-D measurement of soft tissues and bones in musculoskeletal system.

Key words: 3-D ultrasound; ultrasound, MRI, 3-D measurement, musculoskeletal body parts.

Introduction

In medical image analysis, 3-D quantitative measurements of the length, angle, area or volume of organs or lesions is important for accurately understanding the anatomical structures, studying the physiological behaviours of organs or tissues, and then making decisions for clinical applications (Nelson and Pretorius, 1998; Roberts et al. 2000; Grenier et al. 2002). The 3-D measurement is normally conducted within a voxel-based 3-D image, which can be formed by stacking a sequence of parallel 2-D slice images generated conventionally by X-ray CT (Roberts et al. 2000) or MRI (Grenier et al. 2002). High quality cross-sectional images of organs and tissues can be provided by the two medical imaging modalities. However, both of them are expensive and need long imaging time. Moreover, patients have to suffer from the harmful ionizing radiation when scanned by X-ray CT.

Unlike CT and MRI, ultrasound imaging has the advantages of being inexpensive, non-ionizing, non-invasive, and easy to access and operate. Conventional 2-D B-mode ultrasound systems allow the operator to guide the probe over patient's skin and generate the 2-D image of the cross-section of the anatomy below the probe in real time. However, the subsequent analysis is normally limited within a single 2-D image plane. The extended field-of-view imaging technique developed recently allows the sonographer to scan over a large region of body tissues to form a panoramic image using the real-time ultrasound probe (Weng et al. 1997; Cooperberg 2001). The extended field-of-view image provides a useful approach to extend the field-of-view of high-resolution linear array and achieves high accuracy for the distance measurement (Weng et al. 1997, Fornage et al. 2000, Ying and Sin 2005). It has been successfully used in different areas including musculoskeletal

(Lin et al. 1999) and abdominal imaging (Kim et al. 2003). Since extended field-of-view imaging requires the all the images to be scanned along the same plane, the measurement across different planes cannot be achieved using this new approach. On the other hand, more and more attention has been paid to extending the imaging capability of ultrasound by developing 3-D ultrasound systems (Nelson and Pretorius 1998; Fenster et al. 2001; Gee et al. 2003). 3-D ultrasound can be used to construct and visualize the volume data of human anatomies in 3-D and to make quantitative 3-D measurement based on the reconstructed volume. Currently, most manufacturers are offering US equipment with 3-D capability and accurate measurements for clinical use.

Although there are many ways to construct 3-D ultrasound systems (Fenster et al. 2001), freehand imaging has become more and more popular, as it is the cheapest and most flexible approach (Gee et al. 2003). Spatial tracking devices are used in most of the freehand systems to provide the position and orientation of the probe and to achieve acceptable accuracies of measurements. In freehand examinations, the operator holds the probe to scan over the region of interest and a group of B-scans each with spatial information measured by the spatial tracking device are collected and used to construct 3-D volumes. However, the tracking devices used in freehand systems are not ideally suited to routine clinical practice because a carefully controlled scanning environment is not easy to obtain (Gee et al. 2003). Also, errors may be introduced during the volume reconstruction due to the interpolation errors and body motion artifacts during the long scanning period (Rohling et al. 1999; Treece et al. 2003). These errors affect the subsequent measurements of distance, angle, area, and volume of tissues (Nelson and Pretorius 1998). In the freehand 3-D systems previously reported (Barry et al. 1997; Nelson and Pretorius 1998; Fenster et

al. 2001; Gee et al. 2003; Treece et al. 2003; Huang et al. 2005), the 3-D data set of a volume must be first constructed for further quantitative analysis. Therefore, the operators have to wait for relatively long computation time for the volume reconstruction, e.g. 1 min for a volume with 126×103×109 voxels as reported by Huang et al. (2005) and a few minutes as reported by Rohling et al. (1999). The performances of computers have recently been improved significantly and accelerated the computation of complex algorithms. For freehand 3D ultrasound systems, the volume reconstruction has also become faster than before. However, if the anatomical region to be reconstructed is too large, the computation power of the current personal computer is still not enough to generate volumes within a short time. For example, when the 3D measurement between the wrist and the shoulder of a subject needs to be conducted, the whole volume may involve a large number of B-scan images and is time-consuming to be reconstructed. Prager et al. (1999 and 2002) reported a freehand system (Stradx) without the need to construct voxel arrays. They referred the system as "*sequential* freehand 3-D ultrasound" in which the displays and volume estimates could be generated through a sequence of B-scans. Accordingly, the quantitative analyses were able to be performed using original B-scans. In addition, Hata et al. (1997) reported a technique to register the ultrasound images collected by a position-tracked freehand 3-D ultrasound system with MRI/CT images for intra-operative navigation during neurosurgery. The 3-D quantitative measurement based on ultrasound images was not integrated into these intra-operative image-guided navigation systems.

In this paper, we introduced a rapid method to conduct 3-D ultrasonic measurement including distances and angles without the need to construct a volume. Based on a portable freehand 3-D ultrasound system previously developed (Huang et al. 2005), we recorded a

small number of ultrasound images with 3-D spatial localizations and measured the distance and angle of ***interested*** tissues components in the images displayed in the 3-D space. This method allowed rapid quantitative tissue assessment for some applications, such as musculoskeletal modelling and diagnosis (Lieber and Friden 2000), where the spatial relationship between different tissues is essential.

Methods

System overview

A freehand 3-D ultrasound imaging system was previously developed and used for the imaging of musculoskeletal tissues (Huang et al. 2005). As illustrated in Fig. 1, this system included three main components,

- A portable medical ultrasound scanner with a linear probe of 7.5 MHz (Sonosite 180PLUS, Sonosite, Inc., Bothell, WA, USA);
- An electromagnetic spatial sensing device (MiniBird, Ascension Technology Corporation, Burlington, VT, USA) for recording the position and orientation of the probe in real time;
- A PC installed with a digital video capture card (NI-IMAQ PCI/PXI-1411, National Instruments Corporation, Austin, TX, USA), and a custom-designed program for data acquisition, processing, visualization and quantitative analysis.

In this system, the video stream containing a sequence of B-scan ultrasound images was produced by the ultrasound scanner. The video capture card was connected to the video output of the ultrasound scanner through a cable and digitized the video signal in real-time

at 25 frames/sec. Meanwhile, the 3-D position and orientation of the spatial sensor which was attached to the probe of the ultrasound scanner were sensed and transferred to the computer through RS232 serial port. The digitized B-scans and the spatial data read from the spatial sensing device were synchronized during data acquisition and the ultrasound images were displayed by the software on the PC screen with respect to their corresponding 3-D spatial positions and orientations.

Calibration

In order to achieve accurate 3-D localization for each collected B-scan, calibration of this freehand 3-D ultrasound system was conducted. There are normally two kinds of calibration experiments, i.e. temporal calibration and spatial calibration (Treece et al. 2003; Huang et al. 2005). In this study, since only a number of B-scans instead of a continuous sequence were captured, we did not continuously record the B-scans and spatial data in a very high frame rate. Our previous study demonstrated that there was a 4.7±4.4 ms time delay between the ultrasound data stream and the spatial data stream using the portable 3-D ultrasound imaging system (Huang et al. 2005). This time delay could be ignored in the current study, as the ultrasound probe was nearly still when an ***interested*** image was recorded. The purpose of the spatial calibration is to establish the spatial transformation of coordinates from the ultrasound image plane to the spatial sensor. In this study, a cross-wire phantom (Barry et al. 1997) was used for the experiment of spatial calibration. Two cotton wires were crossed in a water tank. In each experiment, around 60 B-scans as well as the corresponding spatial information, were recorded from different directions. The cross was clearly displayed in each of the B-scans. The position of the cross in each B-scan

plane was manually marked and then used to calculate the spatial relationship between the image plane and the spatial sensor using a Levenberg-Marquardt nonlinear algorithm (Prager et al. 1998). In our previous report (Huang et al. 2005), three phantoms with regular shapes were used quantitatively to assess the accuracy of the system. The average errors in three orthogonal directions were 0.1±0.4 mm, -0.3±0.3 mm and 0.3±0.4 mm, respectively.

Data acquisition

During the freehand scanning, the operator could move the ultrasound probe freely over the subject's skin. The captured B-scan images could be displayed in 3-D space with respect to the spatial data stream simultaneously read from the spatial locating device in real time. The B-scan images as well as their 3-D localizations could be observed during examination. If a B-scan contained valuable diagnostic information, it could be recorded with its corresponding spatial information. Usually, more than one B-scan would be recorded for studying the spatial relationships among different tissue components of the ***interested*** body parts, as shown in Fig. 2a. The images of the tissues could be captured in arbitrary directions as long as it was useful for the visualization and analysis. Image processing techniques were also developed to adjust the brightness and the contrast of B-scan images, to remove noise using Median (3×3 or 5×5 pixels) and Gaussian ($\delta = 0.5 – 2.0$, kernel size = 3×3 or 5×5 pixels) filters, and to select region-of-interest (ROI). In addition, the B-scan images could be obtained from multiple body parts for the measurement across different tissue components inside these body parts, such as the forearm and the shoulder.

Quantitative analysis

We developed an interactive function for conducting 3-D measurement of distance and angle, as shown in Fig. 2b. Based on our system, three interactive steps were provided for the measurement. Firstly, the operator could rotate, translate, and scale the collected images in 3-D to select an appropriate view for analysis. During these operations, the whole image set would be adjusted accordingly. Secondly, the 3-D measurement of distance could be performed by clicking point-of-interest on a B-scan plane and dragging a line to another point-of-interest on the same or a different B-scan plane. The distance could be calculated immediately according to the positions of the two selected points. Similarly, the angle between two ***interested*** lines could be obtained by dragging the two lines among those B-scan image planes. The calculation of the angle was given by the following equation:

$$\theta = \arccos\left(\frac{V_1 \cdot V_2}{|V_1| \cdot |V_2|}\right), \quad (1)$$

where, θ is the angle between the two lines in 3-D space, V_1 and V_2 the vectors of the two lines. Thirdly, the images with the added points and lines could be rotated, translated, and scaled for reviewing the results to see whether fine adjustments were acquired. If those points and lines were not correctly selected for the ***interested*** tissues components and the landmarks, they would be adjusted by the operator and new measurement would be conducted by repeating the above three steps.

Validation phantom and experiments

In order to demonstrate the measurement accuracy of this new method, we designed a phantom for the validation experiments. As shown in Fig. 3a, the phantom was comprised of three plastic cylinders with different dimensions. Three holes (radius = 1 mm) were drilled on the surface of each cylinder of the phantom as markers for the length measurement. The dimensional information including the distances between the markers and the angles between different cylinders were first measured by a micrometer. In this paper, three distances (Fig. 3b) were measured among three markers for 5 times on the three cylinders, respectively. The angles between different cylinders were also measured using the approach described as follow. As shown in Fig. 3, the angles between connected cylinders (*A* and *B*, and *B* and *C*) were arranged to be 90° and a protractor was used to measure the exact angles for 5 times. To measure this angle between the two unconnected cylinders *A* and *C*, we placed cylinder *C* parallel to the surface of a flat table and measured the length of *L* and the height of *H* using the micrometer, as indicated in Fig. 3c. The angle could be obtained by calculating the arc tangent of the ratio of *H* and *L*. Five sets of measurements were performed to obtain this angle. In addition, the plastic phantom was placed in a container which was later filled with gelatine (Xilong Chemical Factory, Shantou, Guangdong, China) to mimic the limb joint, as illustrated in Fig. 3d. The cylinders could be assumed to be bones and the gelatine to be soft tissues. In each experiment, three B-scans, in which the three cylinders could be clearly displayed, were acquired (Fig. 3e). 3-D measurement was then conducted using the proposed method. Five sets of measurement were conducted and the results were analyzed. Finally, the measured results were compared with those measured by the micrometer to test the accuracy of the method. The confidence interval of percentage difference between the two measurement

methods was calculated by paired *t*-test at 95% significant level (SPSS, SPSS Inc., Chicago, IL, USA).

In-vivo experiments

Although the implementation of the phantom could provide evidences for the accuracy of this new approach, *in vivo* experiments were important to further demonstrate its usefulness for real applications. In this study, MRI was employed to validate the results measured using our method because of its powerful ability of producing high quality medical images. Blackall et al. (2000) used similar MRI scanning for the calibration of their 3-D freehand US system. It was reported that the geometric accuracy of MRI was about 1 mm (Landi et al. 2001). The lower legs and feet of three young adult subjects (one female was 21 years of age, and the other two males were 24 years and 28 years of age) were scanned by MRI (Fig. 4a) and the ultrasound scanner with the spatial sensor. The results measured from the 3-D MRI data and those measured by ultrasound were then compared. In order to keep the same postures of their lower limbs during both MRI and ultrasound scanning, the subjects wore an ankle-foot orthosis respectively during the experiments, as shown in Fig. 4a. The MRI scans were carried out to cover the lower limbs of the subjects. A water-filled phantom (bottle phantom, GE Healthcare, USA) was scanned together with one male subject as shown in Fig. 4b. The height and diameter of the phantom were 250 mm and 100 mm, respectively. Ten measurements of the height and diameter in different slices obtained from the reconstructed MRI data and the results were compared with the real values to demonstrate the accuracy of the MRI measurement. The measurements on the volume constructed from the MRI data sets were conducted using our

software, by which arbitrary three orthogonal slices could be generated from a 3-D volume (Huang et al. 2005). The ***interested*** points and lines were manually located among the three orthogonal slices. Two operators (Mr. QH Huang and Ms. MH Lu) performed the experiments independently to study the inter-observer variability. The ultrasound scans were conducted in the laboratory of the Hong Kong Polytechnic University, and the MRI scans were performed in the St Paul's hospital. For each subject in each ultrasound test, five sets of B-scan ultrasound image were collected from the ***interested*** portions of the lower limb. In addition, two US tests were conducted for each subject before and after MRI experiments respectively in two different days (3 days apart). The measurement results of the US tests performed by the two operators were used to demonstrate the reproducibility and repeatability of the proposed methods using intra-class correlation coefficient (ICC). The confidential interval for mean difference between US and MRI measurements was calculated using two-sample *t*-tests at 95% significant level (SPSS, SPSS Inc., Chicago, IL, USA). Assuming that the mean of MRI measurements for each subject is the true value, the mean percentage difference between the results of US and MRI measurements were calculated to demonstrate the accuracy of our measurement method.

Results

Validation results

Table 1 presents the results measured by the ultrasound system in comparison with those obtained by the micrometer. The mean error of the distance measurement using the ultrasound method was -0.8±1.7 mm (-2.3±3.6%) and the mean error of the angle measurement was -0.3±2.9° (-0.1±4.1%) at 5% level of significance. It was observed that

the standard deviations are relatively larger in comparison with the means. This could be explained that the ultrasound beam might not perfectly reach the centre of a marker during the scanning. As a result, the measured points in the B-scans were not the real centres of the markers. However, the measured results varied within a small range and the accuracy of this method could be therefore demonstrated.

Results for in vivo experiments

For the bottle phantom, the averaged errors of MRI measurement for the height and diameter were 0.2±1.6 mm and 0.7±1.5 mm, respectively. It was demonstrated that the MRI system could offer good accuracy for the geometrical measurement. Figure 4c shows a 3-D MRI data set (512×512×233 voxels, slice thickness = 2.0 mm) for another subject's lower limbs. The measured parts are also indicated in this figure. For the three subjects, the length of the first metatarsal in the right foot (Fig. 4c) and the angle between the first metatarsal and the middle part of the right tibia measured from the MRI volume were summarized in Table 2. As displayed in Fig. 4c and d, the two bones were not actually in the same plane so that the angle between them could not be measured with a single 2-D image. The B-scans of the subject's right foot and lower leg are shown in Fig. 4d and f, where the distal part of the first metatarsal and the middle part of tibia could be viewed clearly. The comparisons between the results obtained from three MRI volume data sets and those from B-scans are presented in Table 2. It is apparent from the results that the distance was more comparable than the angle. For the three subjects, the differences between US and MRI measurements were -0.8±0.9 mm (-1.2±1.2%), 1.3±1.4 mm (2.4±2.5%), and 0.7±0.9 mm (1.2±1.3%), respectively. The differences in angle

measurement between the US and MRI methods were 1.4±1.7° (2.0±2.5%), 1.4±2.9° (2.3±4.8%), and 2.0±1.9° (3.2±3.1%) at 95% level of significance. With the assumption that the mean values of MRI measurements were true, the overall difference of the length measurement was 0.4±1.3 mm (0.8±2.2%) and that of the angle measurement was 1.6±2.2° (2.5±3.6%)**.** The relatively larger error in angle measurement might be due to the difficulty to maintain the subject's ankle at the exactly same position during the ultrasound and MRI scanning, though the same ankle-foot orthosis was used to fix the subjects' lower limbs.

The repeatability and reproducibility of measurement using the US method are presented in Table 3. It is shown that the US measurement offered low inter- and intra-operator variability in the *in vivo* experiments (ICC > 0.75). The length measurement using the US method had higher ICC values (0.954 and 0.969) indicating very good repeatability and reproducibility, and the angle measurement had relatively lower ICC values (0.795 and 0.891).

Discussion

The main purpose of this paper is to introduce a useful ultrasonic approach for conducting quick 3-D quantitative analysis based on a small number of B-scans, and to preliminary demonstrate its performance using tests on a phantom and three subjects *in vivo*. This approach was realized based on a freehand 3-D ultrasound imaging system. The interactive function developed for the 3-D measurement based on individual 2-D B-scans with spatial information could facilitate the quantitative analysis for many applications. As the creation of voxel arrays were not required using the proposed method, the process of volume reconstruction could be avoided and rapid 3-D measurements of the distance and

angle could be achieved. Experiments were carried out on the validation phantom for evaluating this new approach. In order to test its performance for real applications, MRI scanning was used to validate the measured dimensional information of the lower limb bones of the three subjects. The results of the phantom experiments had shown that the distance and angle measured by the new approach well agreed with those measured by the micrometer with mean error of -2.3±3.6% and -0.1±4.1%, respectively. For the *in vivo* experiments, the differences in the distance and angle measurements using the proposed US method and MRI volume data were 0.8±2.2% and 2.5±3.6%, respectively. The US measurements performed by two operators had shown good repeatability and reproducibility (ICC values > 0.75). The results of the distance measurement presented smaller differences between MRI and US, and better repeatability and reproducibility. It is because the length of the first metatarsal was fixed in different postures of the adult subject while the measured angle might be changed due to the change of the posture when the leg was re-positioned in the ankle-foot orthosis. It was used to keep the subject's posture as the same as possible during the scanning of MRI and ultrasound, which were carried out at two different venues. However, it was noted that even a little rotation of the subject's ankle may result in relatively large difference of the angle between the tibia and the first metatarsal. This issue should be taken into account for the design of future *in vivo* validation experiments.

Another possible error source of the measurement was the procedure of identifying the point or line to represent a selected target in both MRI and B-scan ultrasound images, particularly for the *in vivo* situation. That implied that the measured results might depend greatly on the quality of the raw data and the subjective interpretation of the operator. As

we introduced, several markers were added on the surface of cylinders of the validation phantom in order to locate correct probing direction, along which the markers should be clearly imaged. If the ultrasound beam could not cross the center of the marker, errors could be caused in the subsequent measurement of the distance and angle. Additional errors could be caused in the *in vivo* measurement due to the fact that there is few sharp landmark and subjective judgments for the tissue boundary and landmark are necessary. Such measurement uncertainty also exists in the traditional measurement on single B-scan images or images obtained using extended field-of-view techniques. Similar to the measurement based on extended field-of-view images (Weng et al. 1997, Fornage et al. 2000, Ying and Sin 2005), more comprehensive evaluation of the accuracy and the intra- and inter-operator reliability of this new ultrasonic measurement technique should be conducted using more phantoms and subjects *in vivo* in the future.

Although the distances and the angles could be easily measured, our method could not satisfy all 3-D quantitative analysis for diagnosis. As discussed above, no 3-D volume data was created during the whole experiments. Thus, 3-D measurement for volume, such as volume estimation, was unavailable. Furthermore, the calculation of 3-D area, the segmentation and visualization of 3-D shapes for various tissues, organs, etc., and various volume analyses, such as reslicing and orthogonal slices, were also unavailable using the proposed method. As our previous work (Huang et al. 2005) had addressed the applications based on volume assessment, this paper only focused on real time quantitative analysis for the applications without the need to create volume data. We do not have intention to replace neither 3-D volume imaging nor extended field-of-view imaging using the proposed method. Instead, this approach could fill the gap between the measurement based

on the 3-D volume, which was slow and involves interpolation errors, and that based on the extended field-of-view images or single B-scans, which could not provide measurement across image in different planes or in the 3-D space.

In summary, we presented our recent research work on the 3-D measurement of musculoskeletal body tissues. An approach based on 2-D scans with 3-D spatial information was introduced for a rapid and easy measurement of distances and angles between different tissues. The volume reconstruction was not required using the method and only a small number of useful B-scans with their corresponding 3-D spatial localizations were recorded and used for the measurement. The preliminary phantom validation and *in vivo* experiments demonstrated the accuracy and the performance of this approach. Further systematic evaluations of this approach for the inter- and intro-operator repeatability on more phantoms and subjects are required to demonstrate its clinical values.

Acknowledgements

This work was partially supported by the The Hong Kong Polytechnic University (G-YD42) and the Research Grants Council of Hong Kong (PolyU 5245/03E).

References

Barry CD, Allott CP, John NW, Mellor PM, Arundel PA, Thomson DS, Waterton JC. Three-dimensional freehand ultrasound: Image reconstruction and volume analysis. Ultrasound Med Biol 1997; 23: 1209-1224.

1 Blackall JM, Rueckert D, Maurer CR, Penney GP, Hill DLG, Hawkes DJ. An image
2 registration approach to automated calibration for freehand 3D ultrasound. In: Lecture
3 Notes in Computer Science 2000; 1935: 462-471.
4 Cooperberg PL, Barberie JJ, Wong T, Fix C. Extended field-of-view ultrasound. Seminars
5 Ultrasound CT MRI 2001; 22: 65-77.
6 Fenster A, Downey DB, Cardinal HN. Three-dimensional ultrasound imaging. Phys Med
7 Biol 2001; 46: R67-R99.
8 Fornage BD, Atkinson EN, Nock LF, Jones PH. US with extended field of view: phantom-
9 tested accuracy of distance measurements. Radiology 2000; 214: 579-584.
10 Gee AH, Prager RW, Treece GM, Berman L. Engineering a freehand 3D ultrasound
11 system. Pattern Recogn Lett 2003; 24: 757-777.
12 Grenier PA, Beigelman-Aubry C, Fetita C, Preteux F, Brauner MW, Lenoir S. New
13 frontiers in CT imaging of airway disease. Eur Radiol 2002; 12: 1022-1044.
14 Hata N, Dohi T, Iseki H, Takakura K. Development of a frameless and armless stereotactic
15 neuronavigation system with ultrasonographic registration. Neurosurgery 1997; 41:
16 608-613.
17 Huang QH, Zheng YP, Lu MH, Chi ZR. Development of a portable 3D ultrasound
18 imaging system for musculoskeletal tissues. Ultrasonics 2005; 43: 153-163.
19 Kim SH, Choi BI, Kim KW, Lee KH, Han JK. Extended field-of-view sonography:
20 advantages in abdominal applications. J Ultrasound Med 2003; 22: 385-394.
21 Landi A, Marina R, DeGrandi C, Crespi A, Montanari G, Sganzerla EP, Gaini SM.
22 Accuracy of stereotactic localisation with magnetic resonance compared to CT scan:
23 Experimental findings. ACTA Neurochirurgica 2000; 143: 593-601

1 Lieber RL, Friden J. Functional and clinical significance of skeletal muscle architecture.
2 Muscle Nerve 2000; 23: 1647-1666.
3 Lin EC, Middleton WD, Teefey SA. Extended field of view sonography in musculoskeletal
4 imaging. J Ultrasound Med 1999; 18: 147-152.
5 Nelson TR, Pretorius DH. Three-dimensional ultrasound imaging. Ultrasound Med Biol
6 1998; 24: 1243-1270.
7 Prager RW, Gee AH, Berman L. Stradx: real-time acquisition and visualization of
8 freehand three-dimensional ultrasound. Med Image Anal 1999; 3: 129-140.
9 Prager RW, Gee AH, Treece GM, Berman L. Freehand 3D ultrasound without voxels:
10 volume measurement and visualization using the Stradx system. Ultrasonics 2002; 40:
11 109-115.
12 Prager RW, Rohling RN, Gee AH, Berman L. Rapid calibration for 3-D freehand
13 ultrasound. Ultrasound Med Biol 1998; 24: 855-869.
14 Roberts N, Puddephat MJ, McNulty V. The benefit of stereology for quantitative radiology.
15 Brit J Radiol 2000; 73: 679-697.
16 Rohling RN, Gee AH, Berman L. A comparison of freehand three-dimensional ultrasound
17 reconstruction techniques. Med Image Anal 1999; 3: 339-359.
18 Treece GM, Gee AH, Prager RW, Cash CJC, Berman LH. High-definition freehand 3-D
19 ultrasound. Ultrasound Med Biol 2003; 29: 529-546.
20 Weng L, Tirumalai AP, Lawery CM, Nock LF, Gustafson DE, Von Behren PL, Kim JH.
21 US Extended-field-of-view imaging technology. Radiology 1997; 203: 877-880.

Ying M and Sin MH. Comparison of extended field of view and dual image ultrasound techniques: Accuracy and reliability of distance measurements in phantom study. Ultrasound Med Biol 2005; 31: 79-83.

Figure captions

Fig. 1. Diagram of the freehand 3-D ultrasound system.

Fig. 2. Data acquisition and quantitative analysis. (a) Collected B-scans locating in 3-D space; (b) measurements of the distance and angle in 3-D.

Fig. 3. Validation phantom. (a) The phantom including three plastic cylinders; (b) three distances among three markers on the three cylinders; (c) the angle between cylinder *A* and *C* could be measured by calculating the arc tangent of *H*/*L*; (d) the phantom embedded in the gelatine; (e) the 3-D measurement for the three distances and three angles between different cylinders using captured B-scans.

Fig. 4. In-vivo experiments. (a) A subject's lower leg and foot with the ankle-foot orthosis during MRI scanning; (b) the height and diameter of the bottle phantom scanned with a subject were measured as indicated by two arrows; (c) the angle between the first metatarsal and the middle part of tibia was measured as indicated by the two arrows; (d) the measurements for the length of the first metatarsal and the angle between the first metatarsal and the tibia were conducted using the ultrasound method, as indicated by the arrows; (e) the length of the first metatarsal as indicated by the arrow was measured using MRI volume; (e) the captured B-scan ultrasound images showing the two parts of the metatarsal and the two measurement points indicated by the two dots.

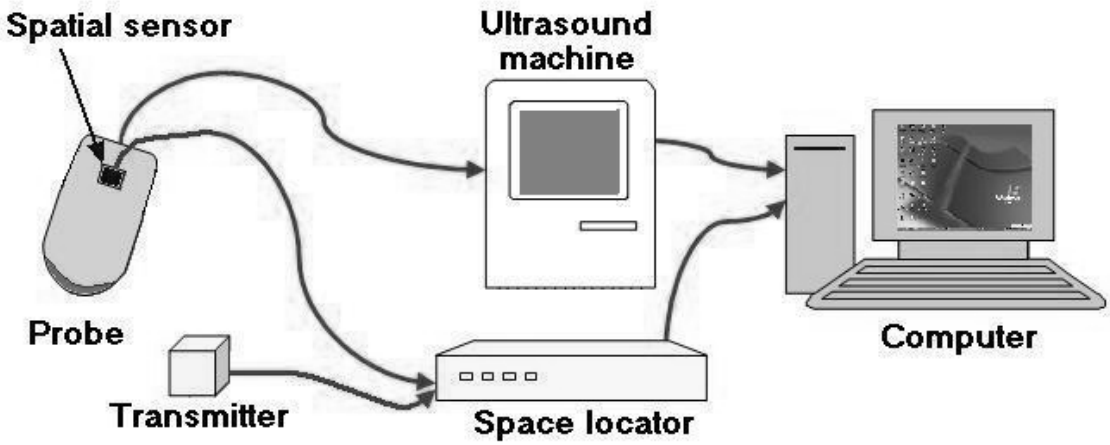
Spatial sensor
Ultrasound machine
Probe
Computer
Transmitter
Space locator

Fig. 1

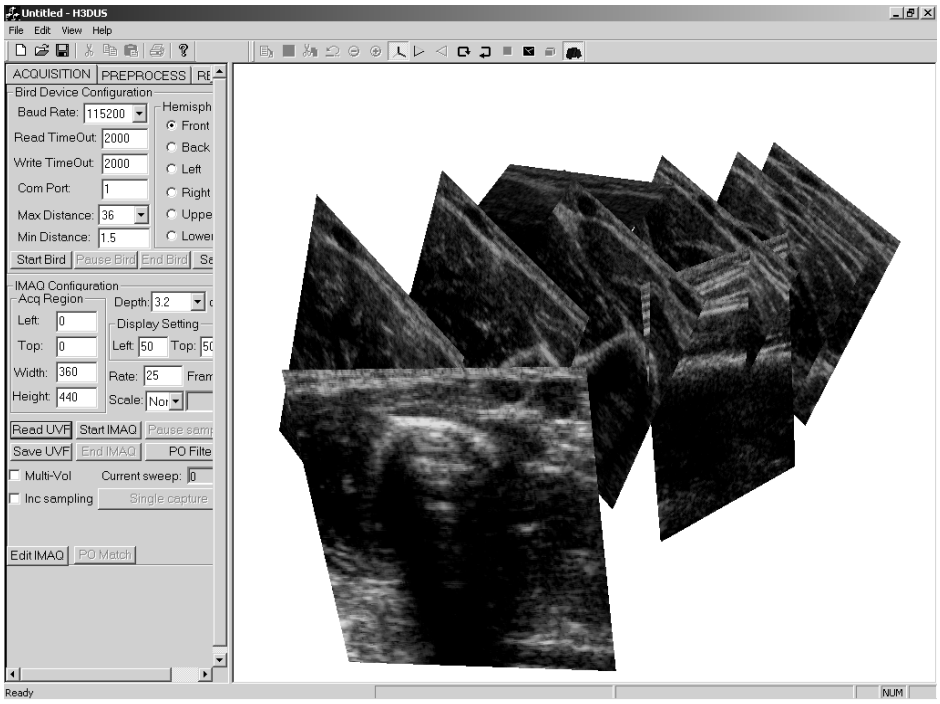
Untitled - H3DUS
File Edit View Help
ACQUISITION
PREPROCESS
Bird Device Configuration
Baud Rate: 115200
Read TimeOut: 2000
Write TimeOut: 2000
Com Port: 1
Max Distance: 36
Min Distance: 1.5
Start Bird
Pause Bird
End Bird
Hemisph
Front
Back
Left
Right
IMAQ Configuration
Acq Region
Left: 0
Top: 0
Width: 360
Height: 440
Depth: 3.2
Display Setting
Rate: 25
Read UVF
Start IMAQ
Save UVF
End IMAQ
Multi-Vol
Current sweep: 0
Inc sampling
Single capture
Edit IMAQ
PO Match
Ready
NUM

Fig. 2(a)

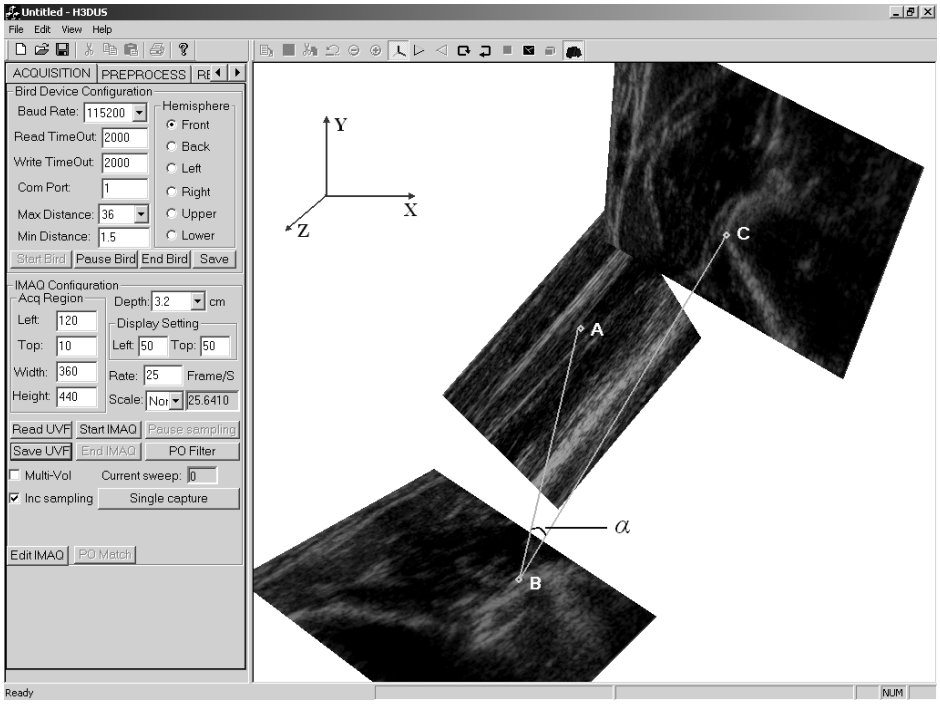
Untitled - H3DUS
File Edit View Help
ACQUISITION
PREPROCESS
Bird Device Configuration
Baud Rate: 115200
Read TimeOut: 2000
Write TimeOut: 2000
Com Port: 1
Max Distance: 36
Min Distance: 1.5
Hemisphere
Front
Back
Left
Right
Upper
Lower
Start Bird
Pause Bird
End Bird
Save
IMAQ Configuration
Acq Region
Depth: 3.2 cm
Left: 120
Top: 10
Width: 360
Height: 440
Display Setting
Left: 50 Top: 50
Rate: 25 Frame/S
Scale: 25.6410
Read UVF
Start IMAQ
Pause sampling
Save UVF
End IMAQ
PO Filter
Multi-Vol
Current sweep: 0
Inc sampling
Single capture
Edit IMAQ
PO Match
Ready
NUM
Y
X
Z
A
B
C
α

Fig. 2(b)

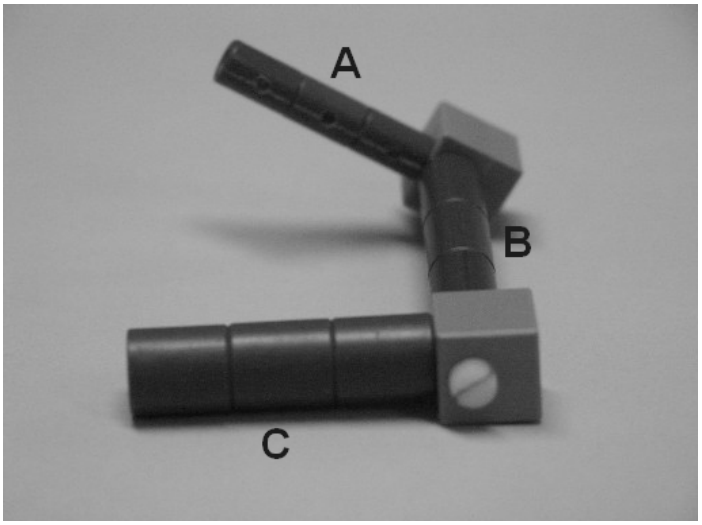
A
B
C

Fig. 3(a)

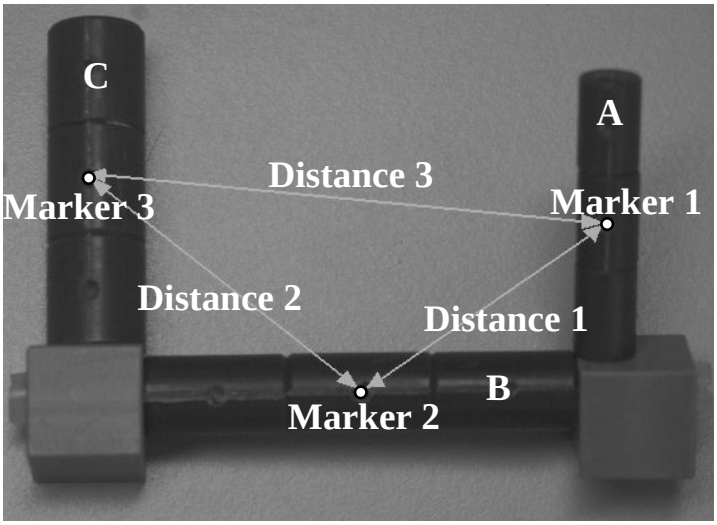
C
A
Distance 3
Marker 3
Marker 1
Distance 2
Distance 1
B
Marker 2

Fig. 3(b)

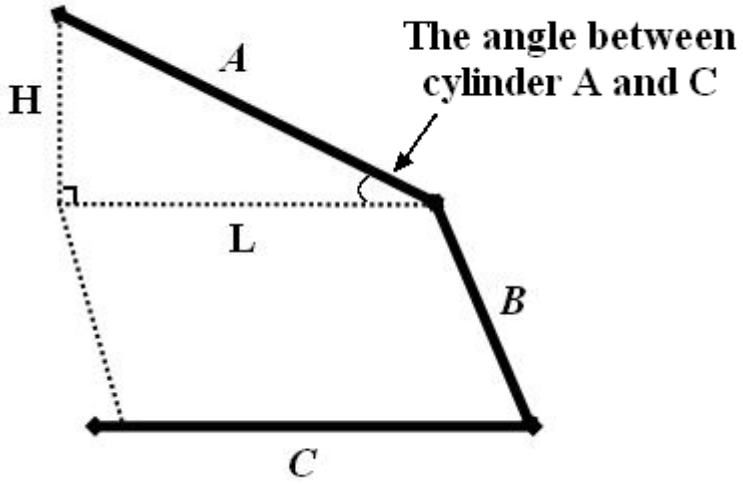
H
A
The angle between cylinder A and C
L
B
C

Fig. 3(c)

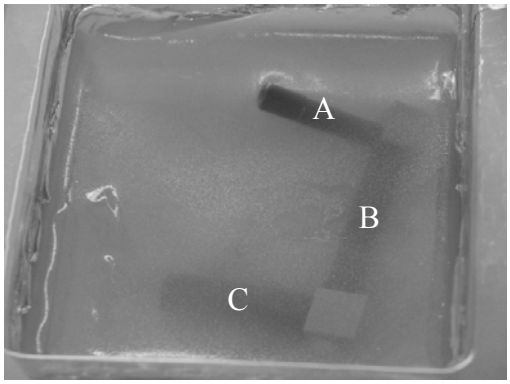

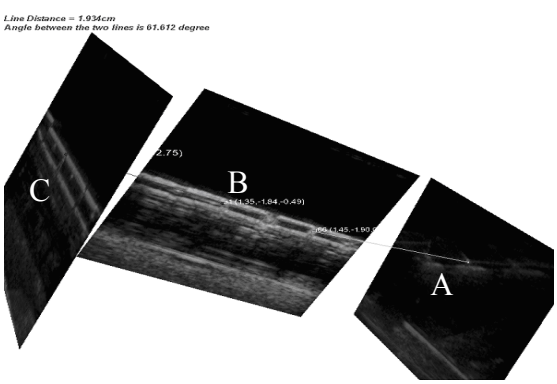

Fig. 3(d) Fig. 3(e)

Fig. 4(a)

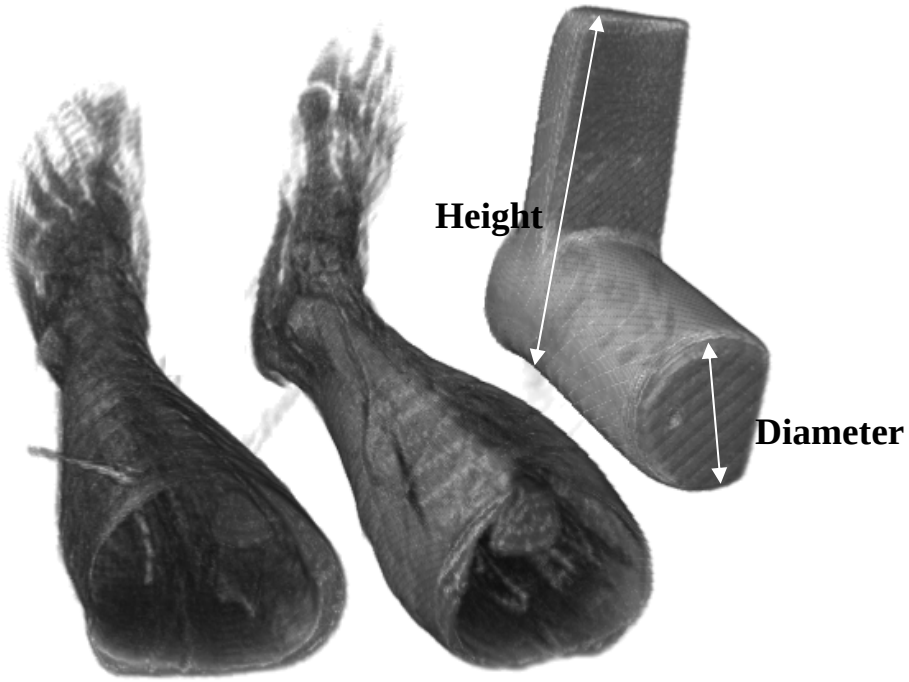

Fig. 4(b)

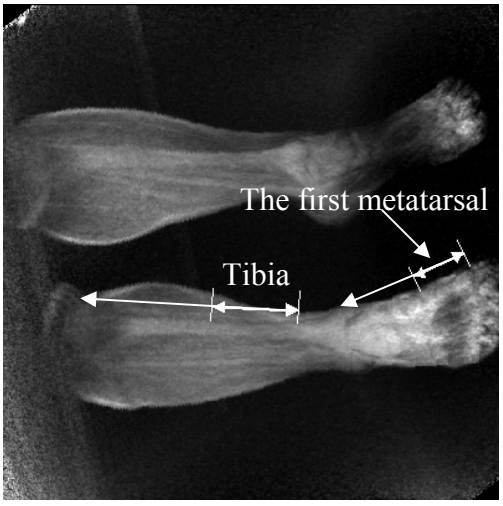

Fig. 4(c)

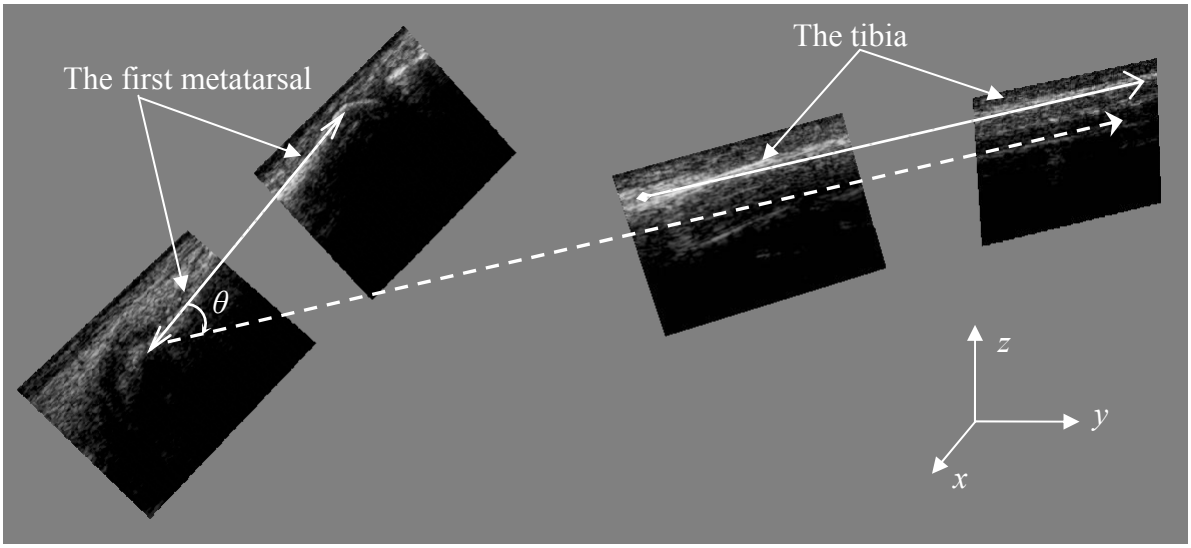

Fig. 4(d)

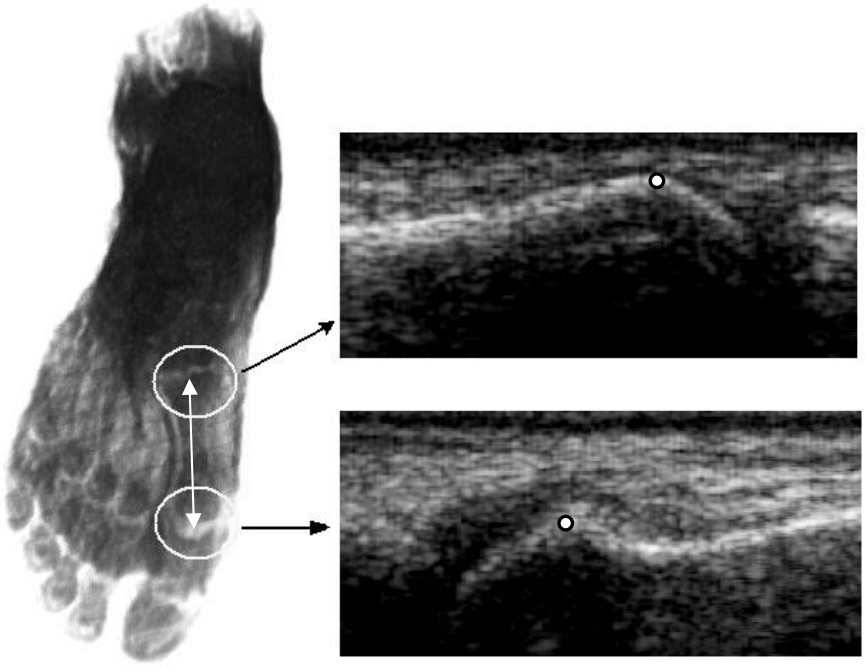

Fig. 4(e)

Fig. 4(f)

Tables

Table 1. Comparison of the results obtained from the validation phantom. Distance 1, 2 and 3 are the three distances labelled in Fig. 3 (b). Angles 1, 2 and 3 denote the angles between cylinder *A* and *C*, *A* and *B*, and *B* and *C*, respectively. The results are presented in mean±SD.

Table 2. Comparison of the measurement results obtained from the three subjects in the *in vivo* experiments. The results are presented in mean±SD.

Table 3. Repeatability and reproducibility of the US measurements.

Table 1.

Measurement	Distance 1 (mm)	Distance 2 (mm)	Distance 3 (mm)	Angle 1 (degree)	Angle 2 (degree)	Angle 3 (degree)
By micrometer	30.4±0.3	36.3±0.3	54.0±0.4	27.2±0.4	90.0±0.2	90.1±0.2
By ultrasound	30.1±1.0	35.0±1.7	53.3±2.2	26.8±1.6	88.9±2.1	92.5±3.8
Confidential interval of Percentage difference at 95% level of significance	(-4.0%, 4.0%)	(-7.8%, 0.5%)	(-6.1%, 1.3%)	(-7.1%, 3.9%)	(-3.3%, 0.9%)	(-1.3%, 6.6%)
Mean percentage difference	Distance: -2.3±3.6%			Angle: -0.1±4.1%		

Table 2.

Measurement	Length of the first metatarsal (mm)			Angle between the first metatarsal and the middle part of tibia (degree)		
	Subject1	Subject2	Subject3	Subject1	Subject2	Subject3
From MRI data	63.4±1.3	53.0±1.5	59.1±1.4	66.3±1.2	58.3±2.5	61.6±1.6
By ultrasound	62.6±0.8	54.3±1.3	59.8±0.8	67.7±1.7	59.7±2.8	63.6±1.9
mean difference at 95% significant level	-0.8±0.9	1.3±1.4	0.7±0.9	1.4±1.7	1.4±2.9	2.0±1.9
Mean Percentage difference	-1.2±1.2%	2.4±2.5%	1.2±1.3%	2.0±2.5%	2.3±4.8%	3.2±3.1%

Table 3

Measurement	ICC of inter-operator variability	ICC of intra-operator variability
Distance measurement	0.969	0.954
Angle measurement	0.891	0.795

ICC = Intraclass correlation coefficient.